Transverse Interferometry of a Hydrogen-Filled Capillary Discharge Waveguide

A. J. Gonsalves,[1] T. P. Rowlands-Rees,[1] B. H. P. Broks,[2] J. J. A. M. van der Mullen,[2] and S. M. Hooker[1]

[1]*Department of Physics, University of Oxford, Clarendon Laboratory, Oxford OX1 3PU, United Kingdom*

[2]*Department of Applied Physics, Eindhoven University of Technology, P.O Box 513, 5600 MD Eindhoven, The Netherlands*

(Received 28 June 2006; published 9 January 2007)

Transverse interferometric measurements are presented of the plasma channel formed in a hydrogen-filled capillary discharge waveguide recently used to generate 1 GeV electrons in a laser-driven plasma accelerator for the first time. The measurements were found to be in good agreement with nonlocal thermal equilibrium simulations, but showed significant differences with the results of a quasistatic model developed by Bobrova *et al.* [Phys. Rev. E. **65**, 016407 (2001)]. The measurements are used to determine scaling laws for the axial electron density and matched spot size of the plasma channel, enabling optimization of the channel to specific applications.

DOI: 10.1103/PhysRevLett.98.025002 PACS numbers: 52.40.Fd, 52.30.Ex, 52.38.Kd

Laser-driven plasma accelerators—in which particles are accelerated by the field of a plasma wave trailing an intense laser pulse—offer the prospect of extremely compact sources of energetic electrons. However, until very recently, the electron energy that could be achieved was limited to the 100 MeV range because it was not possible to maintain the required laser intensity, and hence acceleration, over lengths much more than 1 mm [1–3]. This limitation was recently overcome by employing a hydrogen-filled capillary discharge waveguide: guiding of laser pulses with an intensity in excess of 10^{18} W cm^{-2} through 33 mm of plasma allowed electrons to be accelerated to energies in excess of 1 GeV for the first time in a laser-driven plasma accelerator [4].

For the future development of laser-driven plasma accelerators—and other applications of waveguides for high-intensity laser pulses, such as short-wavelength lasers [5]—it is important to understand in detail the mechanisms by which the waveguide operates and how its properties depend on the external, controllable parameters. For example, decreasing the on-axis electron density in a laser-driven plasma accelerator can increase the energy of the output electron beam by reducing the phase slippage between the relativistic particles and the wake [6]. In this Letter, we address this issue by measuring directly the key guiding properties of the hydrogen-filled capillary discharge waveguide and comparing them with two theoretical models.

The hydrogen-filled capillary discharge waveguide is an example of a plasma waveguide, i.e., guiding is achieved in a plasma column with an electron density which increases with radial distance from the axis. If the transverse electron density profile is of the form $n_e(r) = n_e(0) + (\Delta n_{\mathrm{ch}}/r_{\mathrm{ch}}{}^2)r^2$, a laser pulse with a Gaussian transverse profile will propagate through the waveguide with a constant intensity profile provided that the spot size ($1/e^2$ radius of intensity profile) $w_0 = W_M \equiv (\pi r_e \Delta n_{\mathrm{ch}}/r_{\mathrm{ch}}{}^2)^{-1/4}$ [7], where $n_e(r)$ is the electron density at a distance r from the axis, Δn_{ch} is the increase in density from the axial value at $r = r_{\mathrm{ch}}$, and where r_e is the classical electron radius.

In the hydrogen-filled capillary discharge waveguide the plasma channel is formed by a slow (few hundred nanoseconds) discharge through a gas-filled capillary [8–10]. To date, two groups have investigated the formation of the plasma channel in circular capillaries. Bobrova *et al.* [11] undertook a magnetohydrodynamic (MHD) simulation of the capillary discharge. They found that after an initial period, the electron density profile calculated by the MHD simulation could be approximately reproduced by a simplified quasistatic model (QSM) in which Ohmic heating of the plasma was balanced by heat conduction to the capillary wall. Broks *et al.* used a transient two-dimensional multiregion multifluid nonlocal thermal equilibrium (LTE) model, implemented in the PLASIMO code [12–14]. By performing a parameter study with this model, an empirical relation between the external channel parameters and W_M was obtained [13]. The two models of the capillary discharge were found to give similar values for W_M, but significantly different values of $n_e(0)$.

Given that there are significant differences in the channel parameters calculated by the two models, it is important that these are compared directly with experiment—both so that the dependence of the channel parameters on the controllable parameters is established, and to provide insight into the physics of capillary discharge plasmas. In this Letter, we present the first transverse measurements of the electron density profile formed in a hydrogen-filled capillary discharge waveguide and compare the results with the models of Bobrova *et al.* and Broks *et al.*. The results are summarized in scaling laws for the two key parameters of the waveguide: W_M and $n_e(0)$.

Before describing the present experiments in detail, we note that earlier measurements made in longitudinal geometry were limited to short capillaries (<5 mm) and channels with relatively large W_M by refraction of the probe beam, and may have suffered errors because of the nonuniform regions of plasma at the capillary ends [9].

 © 2007 The American Physical Society

In the experiments described here, these problems were avoided by measuring the density profile transversely. In order to allow for transverse optical access, and to avoid refraction of the probe beam, capillaries of square cross section were formed by sandwiching 2 thinner sapphire plates between two thicker sapphire plates, as illustrated schematically in Fig. 1. The capillaries employed had sides of 125 μm, 210 μm, or 465 μm.

Hydrogen was flowed into the capillary through slots laser-machined into the thick plates. The slots had a cross-sectional area of approximately 0.2 mm^2 and were located 2 mm from either end of the capillary. A capacitance manometer was used to measure the pressure input to the gas slots, and this was cross-calibrated to the pressure inside the capillary as described in Ref. [15].

The discharge circuit—described previously [8]—consisted of a 1.7 nF capacitor charged to a voltage between 11 kV and 30 kV. The discharge was initiated by using a thyratron switch to connect the capacitor across electrodes located at either end of the capillary. The discharge current was measured to be approximately sinusoidal with a half width of 125 ns.

Figure 1 shows schematically the experimental arrangement employed. The capillary was placed in one arm of a Mach-Zehnder interferometer, illuminated simultaneously by 532 nm and 1064 nm pulses of less than 10 ns duration from a Nd:YAG laser. A dielectric mirror was used to direct the 532 nm and 1064 nm laser radiation onto separate CCD cameras, allowing simultaneous two-color interferometry. Virtual wedge fringes in the plane of the capillary were imaged onto the CCD cameras using a lens with a focal length of 75 mm. A third beam (not shown) passed through one of the thick sapphire plates and was reflected off the capillary wall into a separate interferometer. The delay t between the onset of the discharge and the arrival of the probe pulses was varied with a computer-controlled digital delay generator. Fringe patterns were typically recorded at

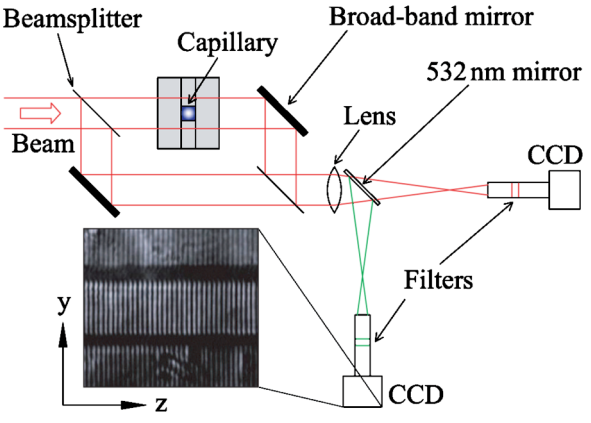

FIG. 1 (color online). The experimental set up used for transverse interferometry measurements of the electron density profile. The inset shows fringes formed in the absence of a discharge by parts of the probe beam passing above, through, and below the capillary channel.

20 ns intervals during the discharge pulse. Measurements of the plasma channel were taken of the main section of the capillary (between the gas injection slots) for initial hydrogen pressures in the range 10 mbar to 150 mbar, with peak discharge currents between 150 A and 600 A.

It can be shown [15] that the refractive index of the plasma inside a hydrogen-filled capillary discharge waveguide is almost completely due to free electrons, and hence the phase shift encoded in the fringe patterns is given by

$$\Phi_p(y, z) = -r_e \lambda \int_{-X/2}^{X/2} n_e(x, y, z) dx, \qquad (1)$$

where λ is the vacuum wavelength of the beam and X is the width of the capillary. The coordinates x, y, and z are the direction of beam propagation, height of the probe beam in the capillary, and distance along the capillary axis, respectively.

However, there is a further contribution to the phase shift experienced by the probe beam: heating of the wall causes an additional phase shift Φ_w by thermal expansion and changes in refractive index such that the measured phase shift is $\Phi_m(y, z) = \Phi_p(y, z) + \Phi_w(y, z)$. Since the temperature-dependent terms of the refractive index do not vary strongly with wavelength [15,16], one can assume $\Phi_w \propto \lambda^{-1}$. Furthermore, since $\Phi_p \propto \lambda$, the phase shift of the probe beam with wavelength $\lambda_1 = 2\lambda_2$ arising from the plasma alone is given by

$$\Phi_p^{\lambda_1}(y, z) = \frac{4}{3}\Phi_m^{\lambda_1}(y, z) - \frac{2}{3}\Phi_m^{\lambda_2}(y, z), \qquad (2)$$

where $\Phi_m^{\lambda_1}$ and $\Phi_m^{\lambda_2}$ are the measured phase shifts at λ_1 and λ_2, respectively. Combining Eqns. (1) and (2), the integrated electron density can be related to the measured phase using

$$\int_{-X/2}^{X/2} n_e(x, y, z) dx = -\frac{2}{3 r_e \lambda}(2\Phi_m^{\lambda_1} - \Phi_m^{\lambda_2}). \qquad (3)$$

Equation (1) shows that if heating of the wall material is negligible, the phase shift at 1064 nm should be twice that at 532 nm. If this is not the case, then Eqn. (3) can be used to calculate the electron density integrated along the x direction. We note that heating of the capillary wall causes negligible ablation (less than 20 pm per shot).

To confirm that changes in the wall material were responsible for cases where $\Phi_m^{\lambda_1} \neq 2\Phi_m^{\lambda_2}$, the phase shift of a probe beam reflected from the capillary wall was also measured. For all the cases where $\Phi_m^{\lambda_1} \neq 2\Phi_m^{\lambda_2}$, a phase shift consistent with the assumptions of Eqn. (2) was observed in the reflected probe beam.

For most of the data collected in this experiment, $\Phi_m^{\lambda_1} = 2\Phi_m^{\lambda_2}$ until several tens of nanoseconds after the peak of ionization, by which time a stable plasma channel had been formed. In such cases, the electron density was deduced using (1). However, this was not always the case for conditions of high-current density, whereupon Eqn. (3) was used to calculate the electron density.

Figure 2 shows the measured phase $\Phi_m(y)$ (averaged over the 2.5 mm range of z recorded by the cameras) at $t = 125$ ns for a capillary of side 465 μm initially filled with 40 mbar of H_2. Also shown is the expected phase variation for the 1064 nm beam calculated by applying Eqn. (1) to the electron density profile $n_e(x, y, z)$ calculated by a non-LTE simulation of Broks *et al.* for a square capillary. It is seen that very good agreement is obtained—well within the errors of the experiments and simulations errors, both estimated to be 20%—apart from the regions close to the capillary wall. The discrepancy in this region is likely due to a combination of refraction of the probe beam by steep density gradients near the wall and the omission of diffusion in the model.

The measurements produce data integrated along the x direction. Reconstruction of the full 3-dimensional electron density profile was achieved by assuming that this satisfies $n_e(x, y, z) = f(x, z)f(y, z)$, where f is to be determined. Within this assumption, the electron density profile is then related to the plasma phase by

$$n_e(x, y, z) = -\left(\frac{1}{r_e\lambda}\right)\frac{\Phi_p(y, z)\Phi_p(x, z)}{\int_{-X/2}^{X/2}\Phi_p(y, z)dy}. \quad (4)$$

The error introduced by this method was assessed by mimicking the reconstruction process on the electron density profile calculated by the non-LTE simulations of Broks *et al.* for the conditions of Fig. 2. The original electron density profile $n_e(x, 0)$ was compared with that obtained by applying Eqn. (4) to the calculated integrated phase shown in Fig. 2. The retrieved electron density profile was found to be in close agreement with the original profile, the error in the deduced matched spot and on-axis density being less than 10%.

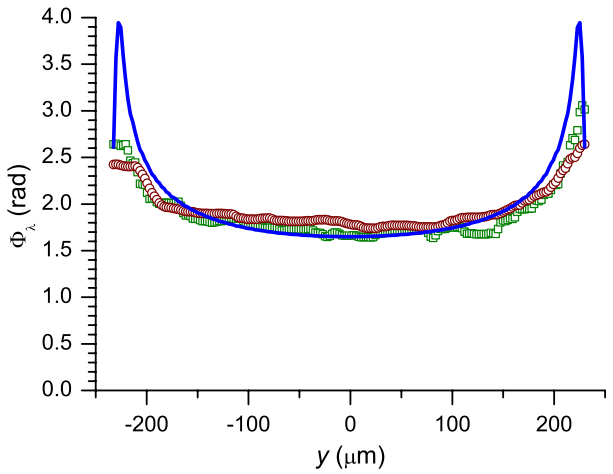

FIG. 2 (color online). Comparison of the measured and simulated phase for a square capillary of side 465 μm, an initial H_2 pressure of 40 mbar, and a peak discharge current of 450 A for a probe wavelength of 1064 nm (circles) and 532 nm (squares). The phase measured by the 532 nm probe has been multiplied by 2 to facilitate comparison. The solid line is that predicted by the non-LTE calculation of Broks *et al.* [14].

The matched spot size of a plasma channel is largely independent of the shape of the electron density profile [17] and is given by the smallest radius r for which the increase in the electron density above the axial value exceeds $(\pi r_e r^2)^{-1}$. This condition was used to determine the matched spot size from the reconstructed electron density profiles as a function of the initial density of hydrogen molecules $n^i_{H_2}$, as shown in Fig. 3 for capillaries of side 465 μm. Also shown are the matched spot sizes calculated for circular capillaries of diameter $D_{cap} = X$ by the QSM (assuming the degree of ionization $Z = 1$) [11] and the scaling law deduced from the non-LTE simulations [13]. Although both of these models strictly apply to capillaries of circular cross section, it has been shown that the shape of the cross section of the capillary has little effect on the electron density profile near the axis, and consequently on the matched spot size [14]. It is seen that the measured matched spot sizes are in very good agreement with the two models, which give similar values for W_M. We note that no significant dependence of the plasma channel on the peak discharge current I was observed for the range of currents employed for this capillary (350 A $< I <$ 650 A), and that Fig. 3 includes all data obtained with the discharge current in this range. The data were not restricted to a constant value of t; instead, channels were analyzed during the period ($t > 80$ ns) when they evolved slowly.

Experiments were also performed using capillaries of side 125 μm and 210 μm. Fitting all the data to a power law gives

$$W_M[\mu\text{m}] = 6.6\times 10^4\left(\frac{X[\mu\text{m}]}{2}\right)^{0.651}(n^i_{H_2}[\text{m}^{-3}])^{-0.1875}. \quad (5)$$

The second important parameter of the plasma channel is the on-axis electron density. This is plotted as a function

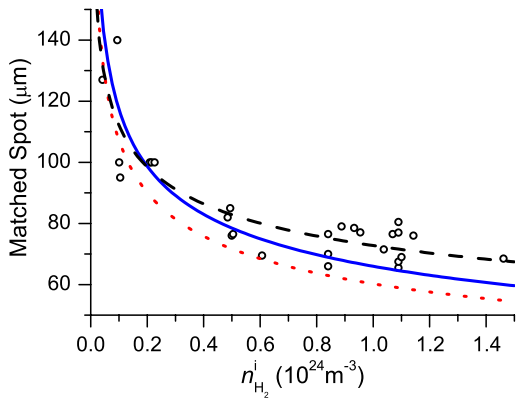

FIG. 3 (color online). Measured matched spot size W_M of the plasma channels formed in capillaries of side 465 μm as a function of the initial density of hydrogen molecules $n^i_{H_2}$. The dotted line shows W_M calculated from the quasistatic model of Bobrova *et al.* and the solid line that deduced from the non-LTE simulations of Broks *et al.*. The dashed line plots the fit given in Eqn. (5).

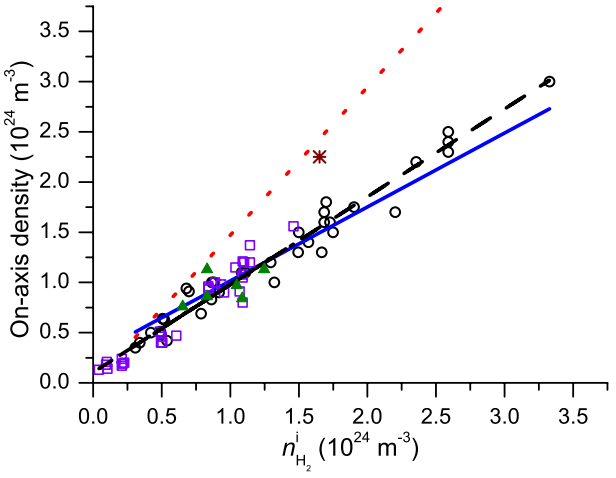

FIG. 4 (color online). The on-axis electron density as a function of initial density of hydrogen molecules for a capillaries of side 125 μm (triangles), 210 μm (circles), and 465 μm (squares). The dotted line shows the on-axis density calculated from the QSM of Bobrova *et al.*, and the solid line that deduced from the non-LTE simulations of Broks *et al.*. The dashed line shows a linear fit to the measured data, and the star denotes the MHD calculation of Bobrova *et al.*.

of $n^i_{H_2}$ in Fig. 4 together with the axial electron densities calculated for circular capillaries of diameter $D_{cap} = X$ by the QSM (assuming $Z = 1$) and the non-LTE simulations. A fit to the measured data yields

$$n_e(0)[\mathrm{m}^{-3}] = 0.87 n^i_{H_2}[\mathrm{m}^{-3}] + 0.11 \times 10^{24}, \qquad (6)$$

as shown in Fig. 4. It can be seen that the axial electron densities calculated by the two models differ significantly for initial hydrogen densities above approximately 1×10^{24} cm^{-3}, and that the measured on-axis electron densities are in remarkably good agreement with the scaling given by Broks *et al.* for circular capillaries [13]. Both the non-LTE simulations and transverse interferometry experiments suggest that the on-axis density rises more slowly with initial hydrogen density than the QSM. This arises from the fact that the plasma is not fully ionized near the capillary wall [13,15]. The on-axis density from the MHD simulation performed by Bobrova *et al.* (star in Fig. 4) also overestimates the on-axis density because in the MHD simulations, heat from the plasma is coupled to free electrons in the wall, leading to a plasma temperature and degree of ionization near the wall which are unphysically high. In contrast, the non-LTE simulations consider the wall an insulator and heat is conducted between the plasma and wall by heavy particles.

In summary, transverse interferometric measurements of the electron density profile of the plasma channel formed in a hydrogen-filled capillary discharge waveguide have been undertaken for the first time. Two key parameters of the plasma channel, the matched spot size W_M and the axial electron density, were compared with those calculated by two models of the capillary discharge. The values of these parameters calculated by the non-LTE simulations of Broks *et al.* were found to be in very good agreement with the measurements; the matched spot size calculated by the quasistatic model of Bobrova *et al.* was also in good agreement with the measurements, but the on-axis electron densities calculated from this model were significantly different from the measured values. This difference is important since the axial electron density is a key parameter of the plasma channel in applications such as laser-driven plasma accelerators. Finally, the measured parameters were used to establish scaling laws for the axial electron density and the matched spot size; these will be useful in tailoring plasma channels for specific applications.

[1] S. P. D. Mangles, C. D. Murphy, Z. Najmudin, A. G. R. Thomas, J. L. Collier, A. E. Dangor, E. J. Divall, P. S. Foster, J. G. Gallacher, and C. J. Hooker *et al.*, Nature (London) **431**, 535 (2004).
[2] C. G. R. Geddes, C. Toth, J. van Tilborg, E. Esarey, C. B. Schroeder, D. Bruhwiler, C. Nieter, J. Cary, and W. P. Leemans, Nature (London) **431**, 538 (2004).
[3] J. Faure, Y. Glinec, A. Pukhov, S. Kiselev, S. Gordienko, E. Lefebvre, J. P. Rousseau, F. Burgy, and V. Malka, Nature (London) **431**, 541 (2004).
[4] W. P. Leemans, B. Nagler, A. J. Gonsalves, C. Toth, K. Nakamura, C. G. R. Geddes, E. Esarey, C. B. Schroeder, and S. M. Hooker, Nature Phys. 2, 696699 (2006).
[5] A. Butler, A. J. Gonsalves, C. M. McKenna, D. J. Spence, S. M. Hooker, S. Sebban, T. Mocek, I. Bettaibi, and B. Cros, Phys. Rev. Lett. **91**, 205001 (2003).
[6] E. Esarey, P. Sprangle, J. Krall, and A. Ting, IEEE Trans. Plasma Sci. **24**, 252 (1996).
[7] P. Sprangle and E. Esarey, Physics of Fluids B, Plasma Physics **4**, 2241 (1992).
[8] D. J. Spence, A. Butler, and S. M. Hooker, J. Phys. B **34**, 4103 (2001).
[9] D. J. Spence and S. M. Hooker, Phys. Rev. E **63**, 015401 (2000).
[10] A. Butler, D. J. Spence, and S. M. Hooker, Phys. Rev. Lett. **89**, 185003 (2002).
[11] N. A. Bobrova, A. A. Esaulov, J. I. Sakai, P. V. Sasorov, D. J. Spence, A. Butler, S. M. Hooker, and S. V. Bulanov, Phys. Rev. E **65**, 016407 (2001).
[12] B. H. P. Broks, K. Garloff, and J. J. A. M. van der Mullen, Phys. Rev. E **71**, 016401 (2005).
[13] B. H. P. Broks, W. van Dijk, and J. J. A. M. van der Mullen, J. Phys. D (to be published).
[14] B. H. P. Broks, W. van Dijk, A. J. Gonsalves, T. Rowlands-Rees, S. M. Hooker, and J. J. A. M. van der Mullen (to be published).
[15] A. J. Gonsalves, T. Rowlands-Rees, B. H. P. Broks, and S. M. Hooker (to be published).
[16] J. Tapping and M. L. Reilly, J. Opt. Soc. Am. A **3**, 610 (1986).
[17] C. G. Durfee, J. Lynch, and H. M. Milchberg, Opt. Lett. **19**, 1937 (1994).